electronics

MDPI

Article

Monitoring Parameters and Optimizing the Technological Process in the Grinding Machine

Grzegorz Śmigielski [1], Małgorzata Łazarska [2] and Mariusz Kaczmarek [1,*]

[1] Faculty of Mechatronics, Kazimierz Wielki University, Kopernika 1, 85-074 Bydgoszcz, Poland; gs@ukw.edu.pl
[2] Faculty of Materials Engineering, Kazimierz Wielki University, Chodkiewicza 30, 85-064 Bydgoszcz, Poland; mlaz@ukw.edu.pl
* Correspondence: mkk@ukw.edu.pl

Abstract: The paper presents the research results related to the operational parameters of a needle grinder for biological materials. The study focused particularly on monitoring the wear of the grinder's working elements, the pins. During the operation of the device, the level and nature of vibrations in the grinding system were examined. In the next stage, after the grinding of 600 tons of biological material, an analysis of the wear of the metal pins was conducted. The degradation process of the pins was observed based on elements made of both untreated steel and heat-treated steel. The apparatus used to measure the grinder's operational parameters consisted of three IEPE KS 80C piezoelectric accelerometers. The applied research methods enabled the identification of vibration components resulting from an improper grinder operation related to pin wear. Based on the conclusions from the conducted research, a low-budget device (prototype) was proposed for continuous machine monitoring, made using an ESP32 system and a capacitive three-axis accelerometer in the MPU6050 system. The applied monitoring method opens new possibilities for quality control and production efficiency in industries that use grinding.

Keywords: wear monitoring; vibrations; vibration descriptors; pin mill grinders; microcontroller in monitoring

check for updates

Academic Editor: Costas Psychalinos

Received: 9 January 2025
Revised: 1 February 2025
Accepted: 4 February 2025
Published: 8 February 2025

Citation: Śmigielski, G.; Łazarska, M.; Kaczmarek, M. Monitoring Parameters and Optimizing the Technological Process in the Grinding Machine. *Electronics* **2025**, *14*, 655. https://doi.org/10.3390/electronics14040655

Copyright: © 2025 by the authors. Licensee MDPI, Basel, Switzerland. This article is an open access article distributed under the terms and conditions of the Creative Commons Attribution (CC BY) license (https://creativecommons.org/licenses/by/4.0/).

1. Introduction

The dynamic development of technology in the industry leads to the improvement of production processes and the implementation of increasingly advanced technological innovations. These actions result in increased efficiency and product quality, as well as more efficient and sustainable resource management. Technological development, including the implementation of automation and robotics, as well as process monitoring, allows for increased efficiency and precision in production. In monitoring, digital transformation plays a key role, encompassing the implementation of Industry 4.0 solutions, such as the Internet of Things (IoT), big data analysis, and artificial intelligence [1–4].

Another important aspect of modern production processes is sustainable development, which includes efficient energy management, the increased use of recycled materials, and minimizing environmental pollution. Grinding organic materials involves reducing the size of particles of organic substances, such as biodegradable waste, plant materials, or industrial organic materials. The efficient grinding of materials poses a significant challenge in various production sectors, such as the food, feed, and waste recycling industries. Problems in such processes arise from factors like the diverse geometric and mechanical properties of biological materials, their high and variable moisture content, or the fat content. The effective grinding of organic materials requires a large amount of

energy, resulting in high operational costs. Additionally, due to the specific properties of the ground materials, the selection of appropriate methods, machines, and optimization of working parameters are crucial. The rapid and uncontrolled wear of machine elements, such as pins, leads to a decrease in the grinding quality and high operational costs. Optimizing the grinding processes and device working parameters reduces costs and increases the operational efficiency, which is important for the long-term use of grinding technology [5–7]. The properties of steel with a specific chemical composition depend on its structure. Heat treatment is applied to improve and shape the mechanical and physicochemical properties of steel to meet operational needs and requirements. This process involves causing structural changes in alloys in the solid state as a result of raising or lowering the temperature of thermally shaped materials. Appropriately selected and conducted heat treatment conditions, in the current state of knowledge, significantly impact the exploitation of finished steel products [8]. Tool steel used for grinding pins is characterized by high wear resistance and the ability to maintain hardness under difficult operational conditions. This steel is primarily used where tools must be highly durable and long-lasting. Due to the high carbon and chromium content in the steel structure, hard carbides form, significantly increasing its wear resistance [9].

In recent years, there has been a growing interest in research on monitoring parameters and optimizing technological processes. One related method used in the diagnostics and operation of various devices is thermography, an infrared imaging technique. It can serve as a tool for the monitoring and proper maintenance of industrial equipment [10]. Infrared thermographic measurements combined with a developed machine learning system enables the prediction of failures in industrial devices. Regular maintenance contributes to the prolonged operation of machines and equipment, enhances their efficiency, reduces the risk of malfunctions, and increases safety during use. Another research approach involves technologies supporting diagnostics and operation. An example of this is the design of methods for improving the quality of thermal images [11,12]. The authors focused on simultaneously reducing noise, enhancing contrast, and preserving details in infrared images. The authors' goal was to develop a synergistic network that integrates these three aspects to achieve better results in thermal image processing.

The primary objective of the research was to develop a new method for monitoring the operation of a biomaterial grinder. The research problem served as an impetus for designing a practical and relatively low-complexity device for the early diagnosis of the wear on the pins mounted in the grinding head of the biomaterial grinder. The paper discusses the successive stages of developing an effective process for monitoring the operation of a universal wide-chamber mill, designed for the fine and very fine grinding of organic materials in needle grinders. These machines ensure high quality of the grinded material and are used in cases where other grinding techniques prove less effective. However, it is worth noting that the literature lacks descriptions of monitoring methods for such machines, where the main problem remains the rapid wear of grinding pins.

2. Research Methodology

2.1. Material Being Ground

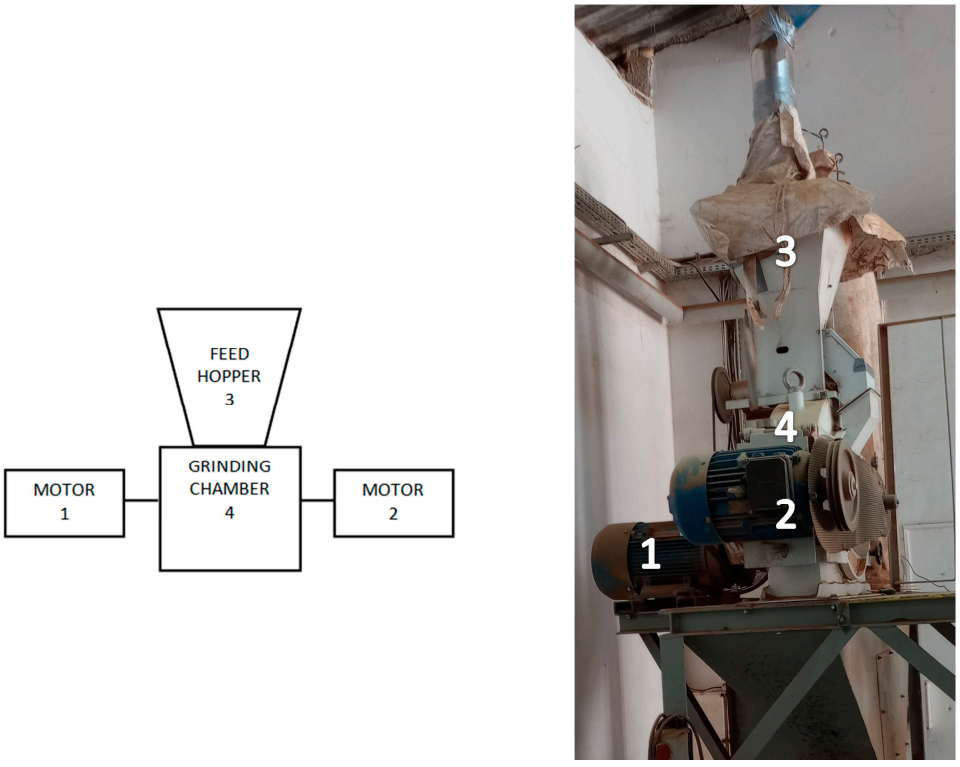
The material ground using the grinder is feed yeast (brewer's yeast). This yeast is a by-product of alcoholic fermentation in beer brewing. Due to its content of protein, B vitamins, and trace elements, it is valued in human and animal diets. In both fresh and dried forms, it contains silicon in small amounts. This element is present in the structure of their cell walls. The average silicon content is about 0.1–0.2 mg per gram of dry mass, although this amount may vary depending on the yeast variety, growing conditions, and processing method. Grinding feed yeast is a technological process that reduces the size

of its particles, allowing its use in dietary supplements, feed production, and the food industry. Yeast is usually grinded after drying, as processing wet yeast is more demanding.

The research was conducted in a company specializing in grinding feed yeast and selling these high-quality, ecological feed additives. Optimizing the grinding process of brewing yeast in terms of reducing the wear of grinding machines requires an understanding of the role of the physical and chemical properties and moisture of yeast in this process. The hypothesis is that minerals present in small amounts in yeast can cause the abrasion of grinding machine elements, and this wear of grinding tools requires detailed research. Current knowledge in this area is insufficient.

2.2. Construction and Operating Principle of the Grinder

The grinder under investigation was constructed by a Polish manufacturer according to the concept developed in the last century by Hosokawa Alpine. The diagram of the grinder is shown in Figure 1a, while its view is in Figure 1b. It is a universal wide-chamber mill designed for the fine grinding of a wide range of products. It is particularly effective for materials containing high amounts of fats, having a sticky consistency, or being sensitive to elevated temperatures.



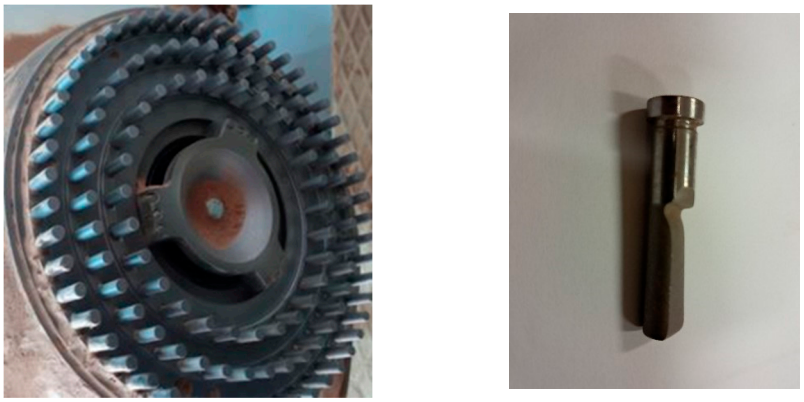
(**a**) (**b**)

Figure 1. Wide-chamber grinder: (**a**) diagram; (**b**) general view.

The crushed material is transported to the feed hopper via a screw conveyor and then into the chamber, where the fragmentation process occurs due to multiple collisions of material particles with moving components.

The working elements in the grinding chamber are two movable discs, equipped with impact pins. One of the discs, located on the door (the hinged flap—Figure 2a), which allows access to the chamber, has 120 pins (arranged in circles of 52, 40, and 28 pieces), while the fixed disc has 108 pins (48, 36, and 24 pieces, respectively). Depending on the type of material and the required degree of the final product size reduction, the discs can operate simultaneously in the same direction, in opposite directions, or one disc can be stationary.

The discs are driven by three-phase motors (OMT-160L-2, OMEC Motors, Arnhem, The Nederland) with a rated power of 18.5 kW and a speed of 2930 rpm, powered directly from the power grid. The disc rotation speed is approximately 3780 rpm. In this particular case, only the drive of one disc (fixed) is used for processing the material. A description of a grinder with a similar, modernized design (Contraplex, Hosokawa Alpine, Augsburg, Germany) can be found on the Hosokawa Alpine website [13].



(**a**) (**b**)

Figure 2. (**a**) View of one of the grinder discs–hinged; (**b**) view of the worn pin.

2.3. Operational Issues

During the operation of the grinder, the pins experience wear (material abrasion), which results in a gradual, yet difficult-to-detect, decrease in efficiency. The complete set of pins must be replaced after grinding approximately 600 tons of material. The decision to replace the pins is based on a visual assessment of their wear. An important aspect related to wear, which has not been fully considered in the operational process so far, is the increase in the imbalance of the discs, which in turn leads to a rise in vibration levels. In the long term, this is a destructive process for the machine, and thus, a timely response is necessary before a drastic increase in vibration levels occurs. Figure 2 shows a view of one of the grinder discs (Figure 2a) and a worn pin (Figure 2b).

For the pins installed in the disc of the studied grinder, NC11LV steel was used. The chemical composition of the steel is presented in Table 1.

Table 1. Chemical composition of NC11LV alloy, element content in wt. %.

C	Si	Mn	Cr	Mo	V
1.53	0.2	0.34	12	0.8	0.95

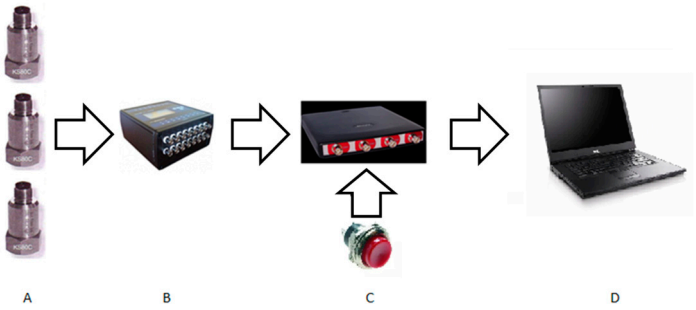
The pins subjected to testing included both raw, non-heat-treated pins and those that underwent heat treatment. NC11LV steel is an alloy tool steel designed for cold work. Due to its high chromium, molybdenum, and vanadium content, it exhibits high wear resistance and hardness. These properties make it an excellent material for manufacturing cutting and forming tools. Additionally, NC11LV steel is characterized by good hardenability and resistance to deformation during the heat treatment process. This ensures the dimensional stability of tools made from this steel. The heat treatment process for NC11LV steel involved heating it to a temperature of 950 °C to homogenize its structure and cooling it in air. After the hardening process, the hardness of the pins was tested using a Rockwell hardness tester.

2.4. Vibration Tests

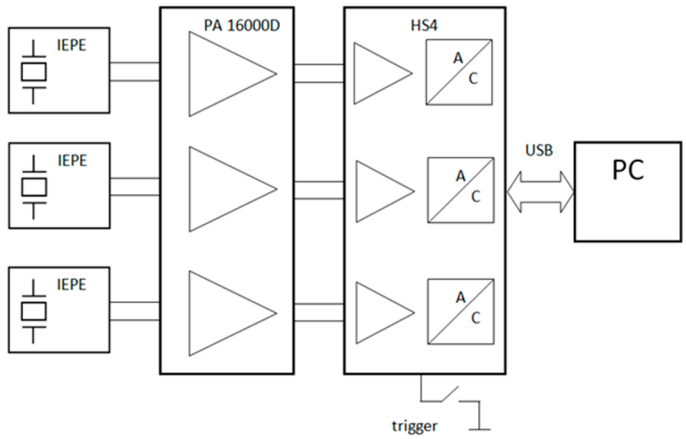
Measurements to determine the level and characteristics of vibrations corresponding to the wear of the pins in the grinding machine were carried out on a machine after several months of operation, during which vibration monitoring had not been implemented. Therefore, the initial state of the machine was unknown. It was assumed that the deterioration of the machine's condition (with cyclic pin replacement) occurs gradually but very slowly, especially compared to the rate of pin wear.

The vibration measurement apparatus consists of three piezoelectric accelerometers (Metra Meß- und Frequenztechnik KS80C) [14], a IEPE signal conditioner (PA 16000D, EC Test Systems, Cracow, Poland), and a 4-channel oscilloscope (Handyscope HS4, Tie Pie, Sneek, The Netherlands) [15] connected to a notebook recording the results using software (Tie Pie Multichannel 1.47.0).

The setup of the vibration measurement apparatus is shown in Figure 3a,b. The applied IEPE-type accelerometers are equipped with a built-in charge amplifier and require only two wires, which serve both as a power supply (with a constant current of 2 to 20 mA) and for transmitting the voltage signal. The sensors were connected via a coaxial cable to the BNC inputs of the signal conditioning system, which provides power to the sensors and amplifies the measurement signals. The connection between the signal conditioner and the 4-channel oscilloscope is also established using a coaxial cable.



(**a**)



(**b**)

Figure 3. Vibration measurement equipment: (**a**) view of components; (**b**) schematic; A—accelerometers KS80C, B—IEPE signal conditioner PA 16000D, C—4-channel oscilloscope Handyscope HS4, D—notebook.

The accelerometers were placed on the casing of the gearbox and the shaft of the fixed disc (X- and Y-axes), as well as on the grinder chamber (Z-axis), as shown in Figure 4. The

selected locations are as close as possible to the moving elements and allow for a mutually perpendicular orientation of the accelerometers.

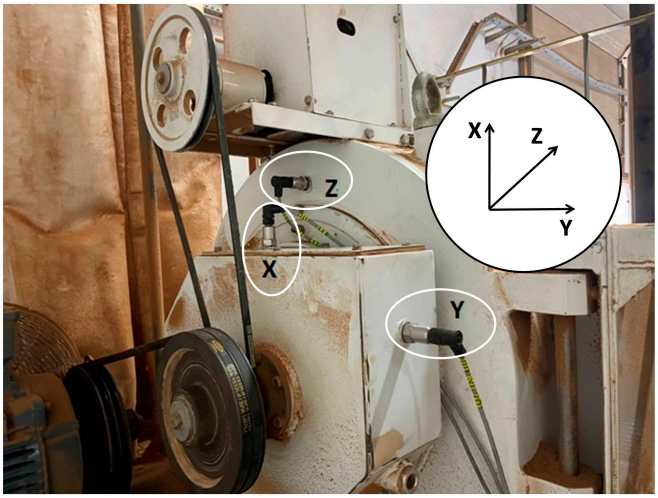


Figure 4. Accelerometer placements on the grinder housing.

Due to the unfavorable measurement conditions (noise, dust), the tests were limited to three measurement series, each 1 s long, with a sampling rate of 100 kS/s. The result files were saved on the computer's disk. The analysis of the results was carried out in an application developed in the LabVIEW environment (National Instruments LabVIEW) [16,17]—Figure 5. The subsequent operations performed by the application include the following:

- loading measurement files;
- signal filtering;
- determining the minimum, maximum, and root mean square (RMS) acceleration values;
- integrating the acceleration signal to obtain vibration velocity and displacement values, as well as calculating the effective values;
- performing a Fourier transform to obtain the frequency spectrum;
- determining the local maxima frequencies for a user-defined detection level;
- analyzing the orders and plotting vibration trajectories for displacement, velocity, and acceleration.

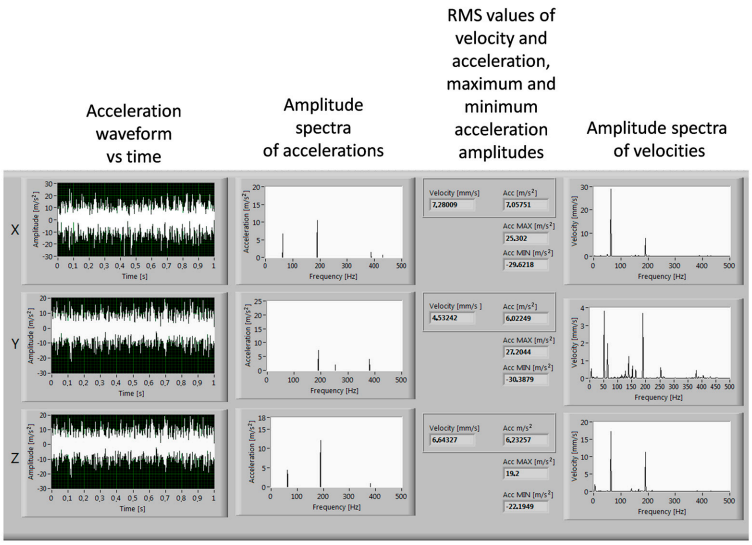


Figure 5. Graphical User Interface of the application.

The user interface of the application, shown in Figure 5, provides the following functionalities (from left): real-time acceleration waveform preview (X-, Y-, Z-axes); spectral analysis results preview (X-, Y-, Z-axes); reading of maximum, minimum, and RMS acceleration values, as well as RMS velocity values (X-, Y-, Z-axes); and spectral analysis results preview for velocity (X-, Y-, Z-axes).

Measurements were conducted for two types of pins (non-hardened and hardened), at two different stages of pin operation (initial and final phases), under idle operation and during grinding. The first measurement for non-hardened pins was performed after grinding 51 tons of material (approximately 9% of the total standard mass processed with one set of pins) and the second after grinding 440 tons of material (approximately 79%). The pin set was replaced after processing 558 tons of material. To ensure comparable conditions, vibration measurements for hardened pins were conducted after processing similar amounts of material—53 tons and 451 tons, respectively. The replacement occurred after 567 tons of processed material.

3. Results of the Research and Discussion

Issues related to imbalance manifest themselves at relatively low vibration frequencies in rotary machines [18,19]. Therefore, low-pass filtering with a cutoff frequency of 500 Hz was applied to the time–domain signals. Due to the expected symptoms of a damaged disc, it can be assumed that the radial directions (X and Y) of the discs with pins are particularly relevant for the analysis. Based on the RMS values of vibration velocities—v_x, v_y, v_z—and accelerations a_x, a_y, a_z obtained from the application for each of the three series of signal acquisitions, mean values, and standard errors of the mean $s(a)$ and $s(v)$ for each axis were calculated.

The value of acceleration recorded by the measurement equipment is expressed by the following relationship:

$$a = \frac{U_2}{K_1 K_2}, \tag{1}$$

where K_1 is the conversion factor from acceleration to voltage of the accelerometer (K_1 = 10.2 mV/m/s^2), U_2 is the voltage measured by the measurement module, and K_2 is the gain of the signal conditioner (K_2= 1).

The uncertainty of acceleration measurement is associated with sensor errors and errors in the signal conditioner and measurement card. The maximum uncertainties of these components were determined based on catalog data: δK_1 = 5%, δK_2 = 0.5%, δU_2 = 0.2%. Partial standard uncertainties are as follows:

$$u(K_1) = \frac{\delta K_1 K_1}{\sqrt{3}}, \tag{2}$$

$$u(K_2) = \frac{\delta K_2 K_2}{\sqrt{3}}, \tag{3}$$

$$u(U_2) = \frac{\delta U_2 FS}{\sqrt{3}}, \tag{4}$$

where FS is maximum reading. The correction by the $\sqrt{3}$ factor arises due to the use of maximum values (assuming that the instrument error follows a rectangular distribution).

The combined uncertainty was estimated using the law of propagation of uncertainty [20,21]:

$$u(a)_{app} = \sqrt{\left(\frac{\partial a}{\partial K_1}\right)^2 u^2(K_1) + \left(\frac{\partial a}{\partial K_2}\right)^2 u^2(K_2) + \left(\frac{\partial a}{\partial U_2}\right)^2 u^2(U_2)}. \tag{5}$$

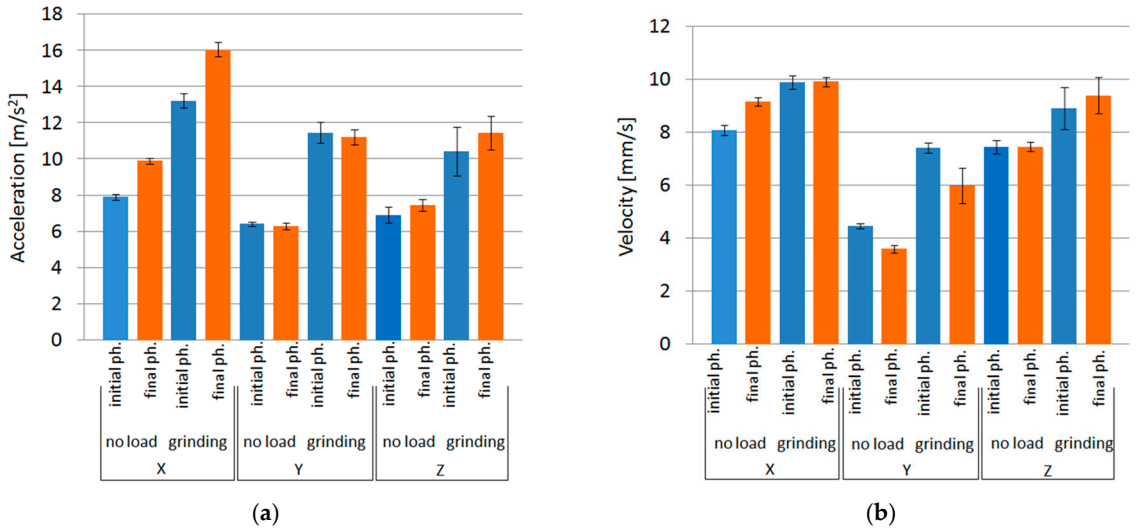
The absolute uncertainty for the maximum measured voltage of 1 V, corresponding to an acceleration of 98 m/s^2, at a full scale (FS) of 1 V is 2.85 m/s^2. The relative uncertainty $u(a)_{rapp}$ = 2.9%, and this relative uncertainty value can also be assumed for the vibration velocity, $u(v)_{rapp}$, since the systematic error of the apparatus (from catalog notes) is constant and proportional to the acceleration, and its impact on the result increases linearly, maintaining the relative error value.

Subsequently, the total measurement uncertainty, including random error from the series of measurements (standard uncertainty)and the instrument error (systematic uncertainty), was calculated.

For acceleration, the total uncertainty is as follows:

$$u_c(a_{avg}) = \sqrt{(u(a_{avg}))^2 + \left(u(a_{avg})_{rapp} a_{avg}\right)^2} \quad (6)$$

The RMS values of accelerations and velocities for discs with non-hardened pins, with uncertainties determined according to the relationships presented above, are shown in Figure 6a,b.



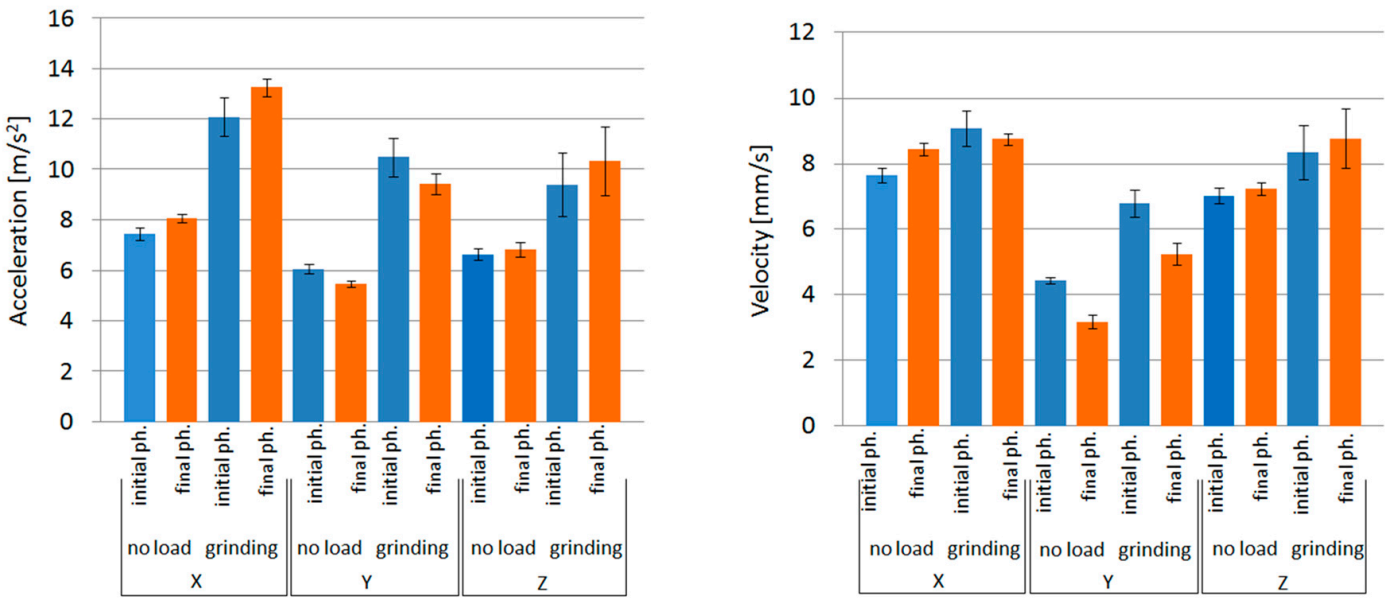
(**a**) (**b**)

Figure 6. (**a**) Acceleration values and (**b**) velocity values for discs with non-hardened pins.

For non-hardened pins in a more advanced wear state, acceleration values in the X-axis significantly increase (from 7.9 m/s^2 to 9.9 m/s^2 during idle operation and from 13.3 m/s^2 to 16 m/s^2 during grinding), while acceleration in the Z-axis slightly increases (from 6.9 m/s^2 to 7.5 m/s^2 and from 10.4 m/s^2 to 11.4 m/s^2, respectively). In contrast, acceleration in the Y-axis slightly decreases (from 6.4 m/s^2 to 6.3 m/s^2 and from 11.5 m/s^2 to 11.2 m/s^2).

In terms of velocity, an increase can also be observed in the X-axis (from 8.1 mm/s to 9.2 mm/s during idle operation and from 9.8 mm/s to 9.9 mm/s during grinding) and in the Z-axis (from 7.4 mm/s to 7.5 mm/s and from 8.9 mm/s to 9.4 mm/s, respectively), while a decrease is observed in the Y-axis (from 4.5 mm/s to 3.6 mm/s and from 7.3 mm/s to 6 mm/s).

The values of accelerations and velocities for discs with hardened pins are presented in Figure 7a,b.



(**a**) (**b**)

Figure 7. (**a**) Acceleration values and (**b**) velocity values for discs with hardened pins.

For the hardened pins in a more advanced state of wear, there is a significant increase in acceleration values in the X-axis (from 7.5 m/s^2 to 8.1 m/s^2 during idle operation and from 12.1 m/s^2 to 13.3 m/s^2 during grinding) and a slight increase in the Z-axis (from 6.6 m/s^2 to 6.8 m/s^2 and from 9.4 m/s^2 to 10.3 m/s^2), while acceleration in the Y-axis slightly decreases (from 6.1 m/s^2 to 5.5 m/s^2 and from 10.5 m/s^2 to 9.4 m/s^2).

In terms of velocity, an increase is also observed in the X-axis (from 7.6 mm/s to 8.4 mm/s during idle operation and from 9.1 mm/s to 8.7 mm/s during grinding) and in the Z-axis (from 7 mm/s to 7.2 mm/s and from 8.3 mm/s to 8.8 mm/s), while a decrease is observed in the Y-axis (from 4.4 mm/s to 3.2 mm/s and from 6.8 mm/s to 5.2 mm/s).

Summarizing the results obtained for the effective values of accelerations and velocities for both hardened and non-hardened pins, a significant increase in acceleration (and velocity) values in the X-axis and a slight increase in the Z-axis can be observed, along with a decrease in acceleration (and velocity) values in the Y-axis. Thus, a difference between the acceleration (and velocity) values in the radial directions X and Y becomes evident. For accelerations, these differences are as follows:

- for non-hardened pins during idle operation—1.5 m/s^2 in the initial phase and 3.6 m/s^2 in the final phase; during grinding, respectively—1.8 m/s^2 and 4.8 m/s^2;
- for hardened pins during idle operation—1.4 m/s^2 in the initial phase and 2.6 m/s^2 in the final phase; during grinding, respectively—1.6 m/s^2 and 3.9 m/s^2.

It is noteworthy that the acceleration differences for hardened pins are smaller than for non-hardened pins, which may indicate a lower degree of wear of the pins.

The acquired acceleration and velocity signals over time were subjected to a frequency analysis to compare the amplitude spectra. For non-hardened pins, the acceleration and velocity spectra are shown in Figure 8a–d.

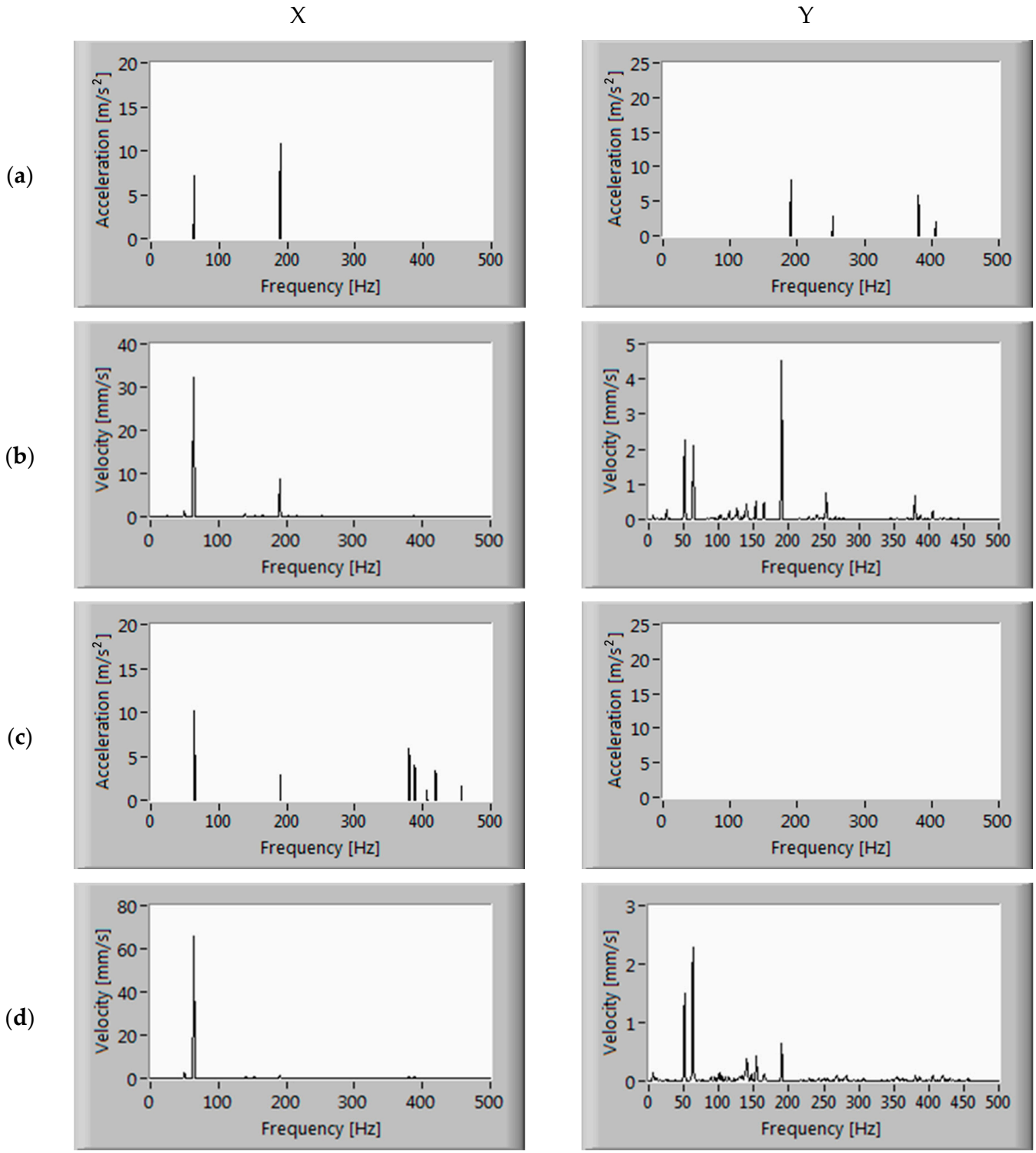


Figure 8. Amplitude spectra of accelerations and velocities for the machine with non-hardened pins (left: X-axis, right: Y-axis): (**a**) accelerations, initial phase, idle operation; (**b**) velocities, initial phase, idle operation; (**c**) accelerations, final phase, idle operation; (**d**) velocities, final phase, idle operation.

A similar analysis was performed for the pins subjected to heat treatment (hardened pins). The results in the form of the amplitude spectra for acceleration and velocity are shown in Figure 9a–d.

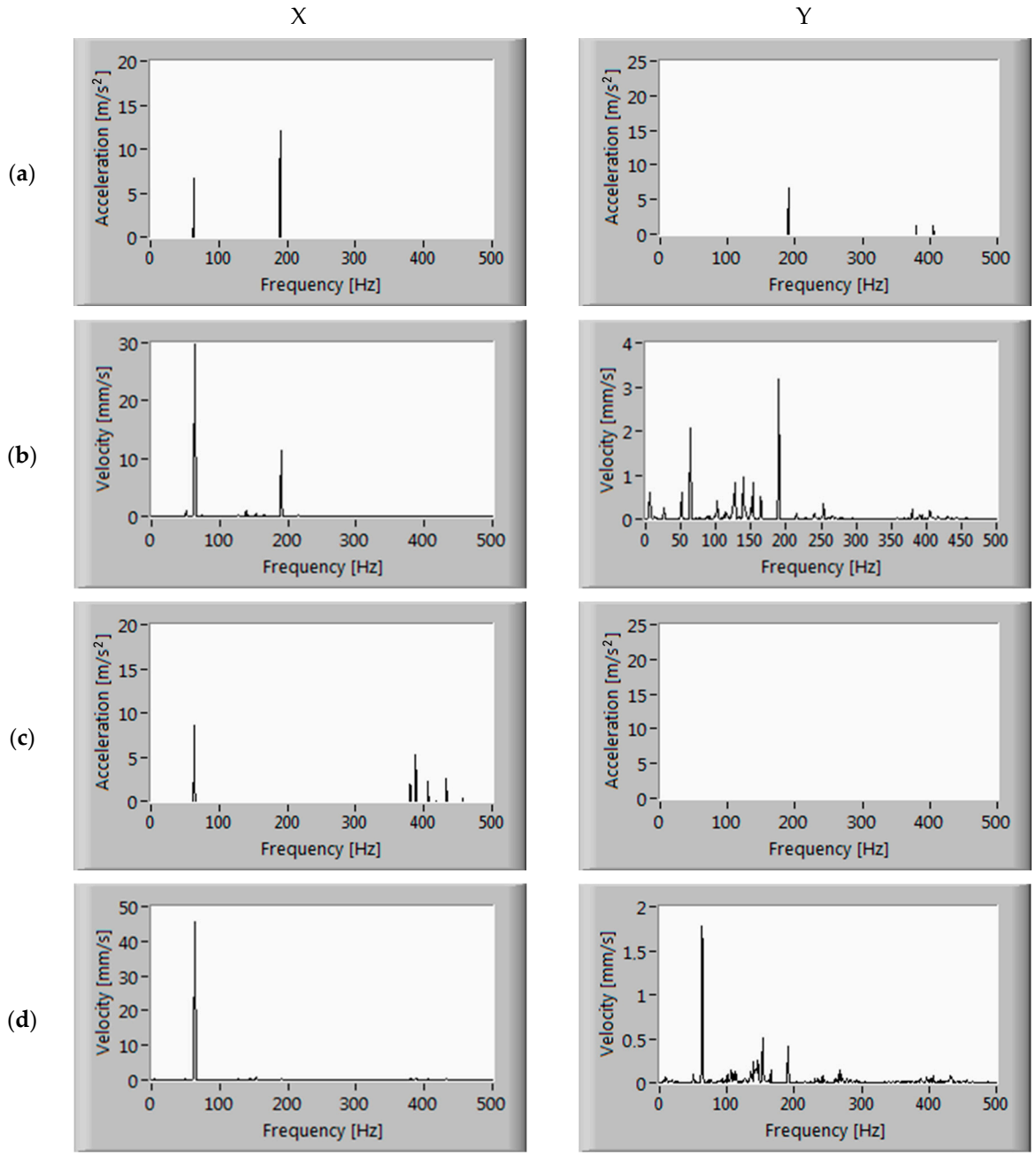


Figure 9. Amplitude spectra of accelerations and velocities for the machine with hardened pins (left: X-axis, right: Y-axis): (**a**) accelerations, initial phase, idle operation; (**b**) velocities, initial phase, idle operation; (**c**) accelerations, final phase, idle operation; (**d**) velocities, final phase, idle operation.

The amplitude spectra for the machine with non-hardened pins are similar to those for the machine with hardened pins. For the velocity signal in the X-axis, a prominent peak at 63 Hz is also observed. In the initial phase, it has a value of approximately 30 mm/s for both non-hardened and hardened pins, while in the final phase, it reaches about 46 mm/s for hardened pins and 65 mm/s for non-hardened pins. The 63 Hz frequency corresponds to the rotational speed of the disc with pins, and the increase in the vibration velocity at this frequency may indicate increased unbalance of the disc. This is clearly visible for the non-hardened pins, which exhibited greater wear at the same stage of the production cycle. The amplitude spectra of velocity in the Y-axis have similar values for the initial and final phases. In the spectrum for the initial phase, for both acceleration and velocity in both axes, a peak at 189 Hz (three times the fundamental frequency) is observed. For

the Y-axis velocity, it has the highest value. In the final phase, it is only visible in the Y-axis velocity signal. In both the first and second cases, additional spikes around the frequency of 380 Hz appear in the final phase. This is likely the sixth harmonic of the fundamental frequency, and its appearance may indicate a change in the nature of the vibrations. Peaks at frequencies of 50 Hz, 100 Hz, and 150 Hz with small amplitude values are also present, likely resulting from the mains frequency and not originating from mechanical vibrations.

The results of the conducted frequency analyses show that for assessing the wear of the pins, the spectrum obtained during idle operation of the grinder is much more significant than during the load. The spectra from the measurements during grinding are similar but contain significantly more frequency bands, making them less readable due to the complex interaction of the pins and grinder disc with the material being ground.

One of the tools used for visualizing and analyzing the dynamic behavior of mechanical systems is phase trajectory analysis in the X–Y-axes for acceleration, velocity, and displacement. Figure 10 shows their comparison for the initial and final phases for the machine with hardened pins.

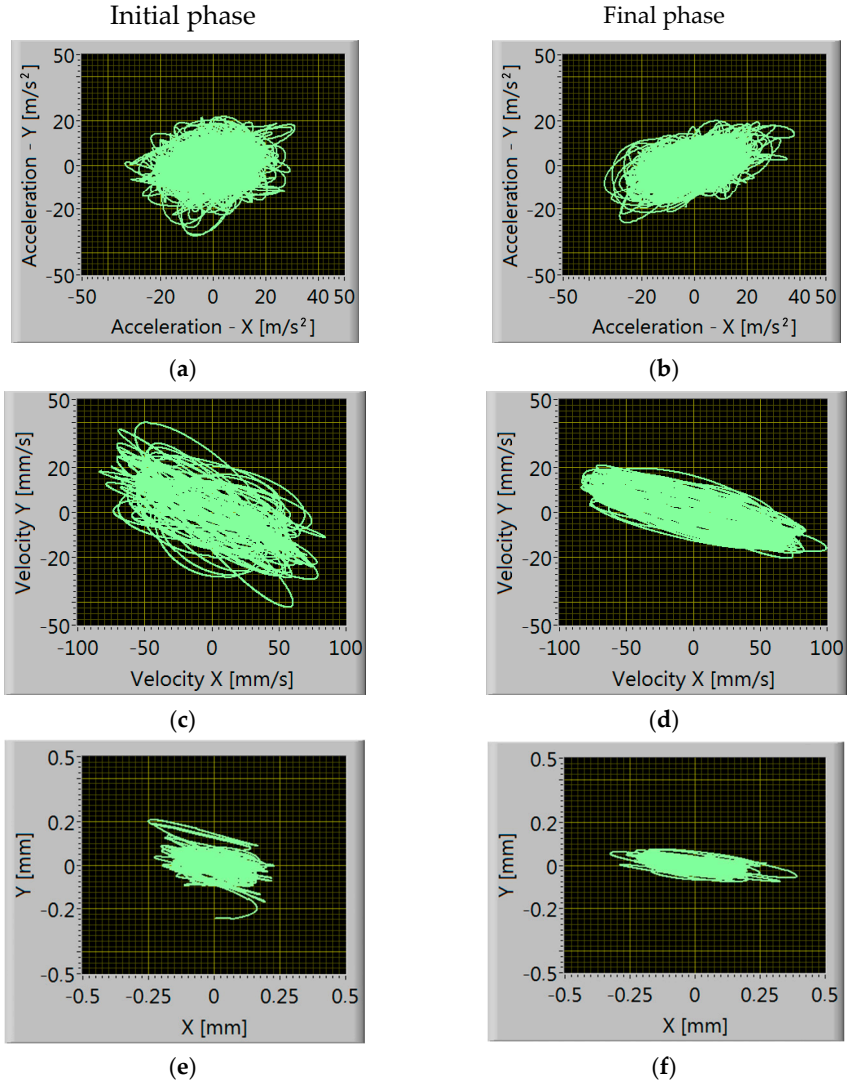


Figure 10. Phase trajectories of vibrations—(**a**) initial phase, acceleration; (**b**) final phase, acceleration, (**c**) initial phase, velocity; (**d**) final phase, velocity; (**e**) initial phase, displacement; (**f**) final phase, displacement.

Comparing the phase trajectories for the initial and final phases, a noticeable elongation in the X-axis for the final phase can be observed, confirming the previously noted trends of the increased vibration intensity in this direction.

Considering that the wear of the grinder disc elements manifests most clearly through an increase in the difference in the RMS values of acceleration and vibration velocity in the X- and Y-axes, and since accelerations are easier to measure as a single-parameter measure of wear, it is worth considering the parameter τ, defined as the ratio of the difference in accelerations in the X- and Y-axes to the smaller of these values:

$$\tau = \frac{a_{xavg} - a_{yavg}}{MIN(a_{xavg}, a_{yavg})} \quad (7)$$

The values of the wear coefficient τ for all measurement series are presented in Table 2.

Table 2. The wear coefficient τ.

Symbol	τ
non-hardened pins	
initial phase	
no load	0.23
grinding	0.15
final phase	
no load	0.57
grinding	0.43
hardened pins	
initial phase	
no load	0.23
grinding	0.15
final phase	
no load	0.48
grinding	0.40

In the initial phase, the τ coefficient for both hardened and non-hardened pins has the same values. In the final phase, the coefficient almost doubles, ranging from 0.4 to 0.57 regardless of the operating mode, which allows it to be used as a descriptor of the pins' condition. The greater wear of non-hardened pins was confirmed by the pin mass measurements, the results of which are presented in Table 3 and in the histogram (Figure 11). The masses of the pins from a new set and the hardened and non-hardened pins after the entire production cycle (after replacing with a new set) were compared.

Table 3. Characteristics of pin masses of the grinder made from NC11LV steel.

	New Pins	Hardened Pins	Non-Hardened Pins
Mean mass [g]	10.75	9.18	8.36
Root mean square error [g]	0.07	0.90	0.55
Minimum mass [g]	10.56	8.25	5.16
Maximum mass [g]	10.89	10.13	9.88
Total mass of the set [g]	2449.76	2093.02	1905.4

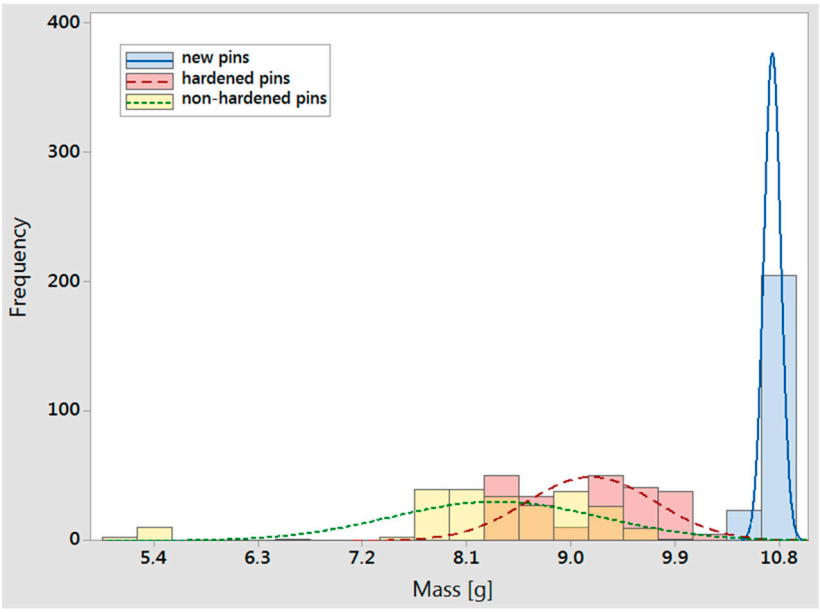
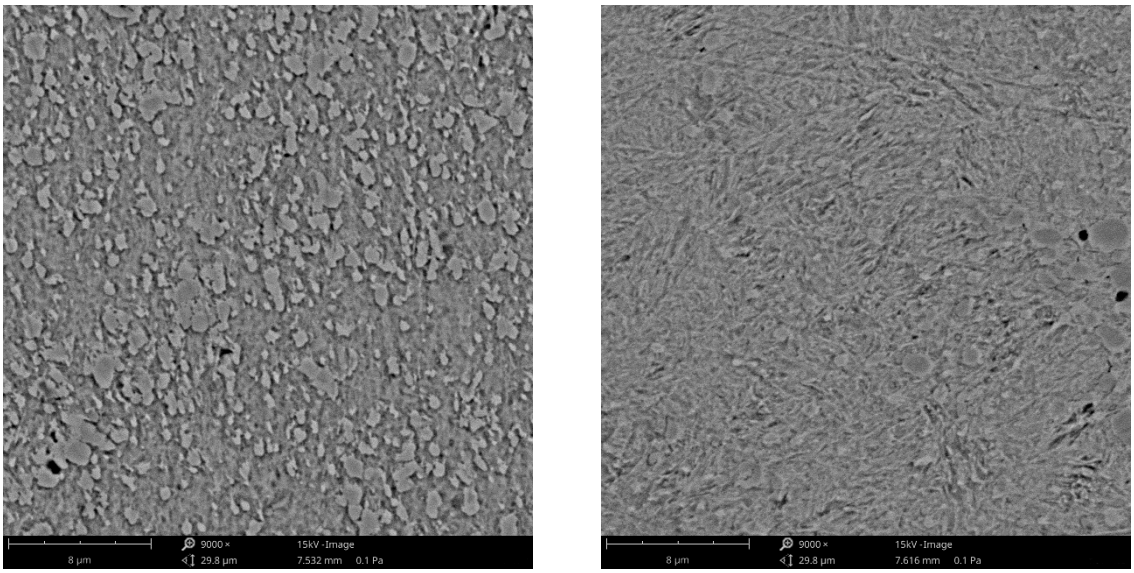


Figure 11. Histogram of pin masses: comparison among new, hardened, and non-hardened pins.

To illustrate the causes of differences in the wear of grinder pins, an analysis of the microstructure of NC11LV steel was conducted before and after heat treatment. Measurements were carried out using a Phenom XL (Thermo Fisher Scientific, Waltham, MA, USA) scanning electron microscope after appropriate processing and etching. The results are presented in Figure 12.



(**a**) (**b**)

Figure 12. Microstructure images of NC11LV tool steel: (**a**) as-received, non-hardened; (**b**) after air hardening.

In its initial state, NC11LV steel exhibits a ferrite–pearlite structure. After hardening, it can be observed that the main component of the matrix is martensite [22]. This phase is characterized by high hardness. Small amounts of retained austenite can also be observed. Additionally, the hardness of the steel after hardening was tested using a Rockwell hardness tester. This is a hard and brittle phase that imparts high hardness to the steel (60 HRC).

4. Proposal for a Device Monitoring Pin Wear

The tested grinder operates efficiently even at very high levels of vibration, but the lack of the timely replacement of working elements—discs and/or pins—leads to rapidly progressing degradation of the entire drive system (bearings, shaft). Consequently, costly and time-consuming machine repairs occur. Examples of such failures in a similar machine have been presented in another article [7]. As mentioned in the introduction, in the current operation of the grinder, determining the appropriate moment for pin replacement is based on a subjective assessment of their wear after opening the grinder chamber. This is not a method based on objective indicators, and additionally, it requires a significant amount of employee time for such activities. Given the above, a low-cost device for continuous monitoring of the machine's condition was designed as part of the project. The prototype device, designed to be mounted directly on the grinder's body, was built using the ESP32 SoC platform (Espressif Systems, Shanghai, China) [23] and a three-axis capacitive accelerometer integrated into the MPU6050 chip (InvenSense, San Jose, CA, USA) [24], along with a simple user interface consisting of two LED indicators and a button. The ESP-based module communicates with the MPU6050 module via the I2C bus. The device is powered by a power bank, with an option for charging from a mains adapter. The block diagram of the device is shown in Figure 13.

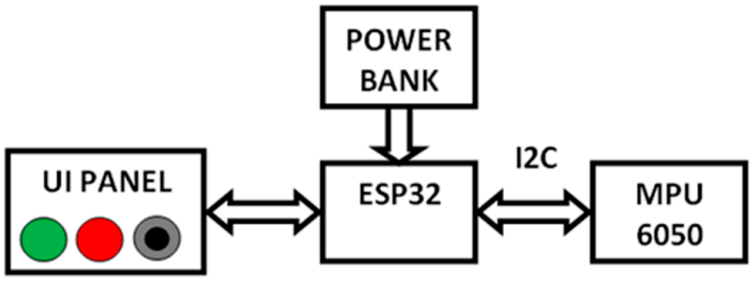


Figure 13. Block diagram of the prototype device for continuous machine condition monitoring.

Based on the conducted tests, it was found that as wear increases, the acceleration value in the X-axis grows, while the acceleration value in the Y-axis decreases, thus the difference in acceleration values between the X- and Y-axes increases. The device enables the measurement of accelerations along the X-, Y-, and Z-axes, the calculation of RMS values for these quantities, and the determination of the τ coefficient (according to Equation (7)). A red LED indicator signals when τ exceeds the threshold set at 0.4.

Independently, exceeding the acceleration value in any axis above a defined threshold (initially set at 17 m/s^2 based on preliminary data) is signaled by a flashing green LED. A button on the user panel enables sensor calibration and alarm reset. Acceleration values can be read remotely. The ESP system has WiFi communication capabilities, but due to the absence of such a network in the production hall, it was configured in access point mode. Access to RMS acceleration data and information on τ threshold exceedance is available via a web browser—Figure 14 [25].

The device was tested in a laboratory vibration measurement setup and handed over for testing and operation at the company's premises. Figure 15 shows photos of the prototype device and its mounting location on the grinder housing. The ESP module with its power supply (1) and the accelerometer module (2) are housed in separate enclosures, made using 3D printing technology. The device enclosure is attached to the grinder housing with a screw, while the accelerometer module enclosure is mounted using a strong magnet.

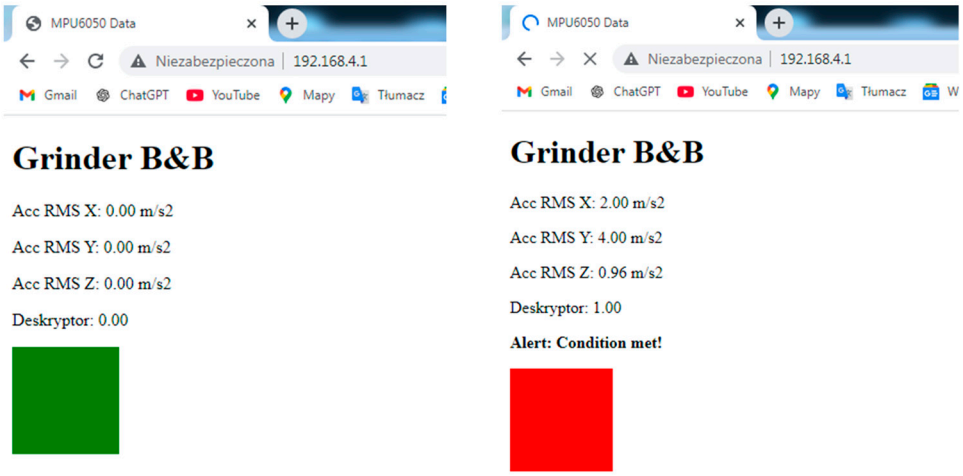
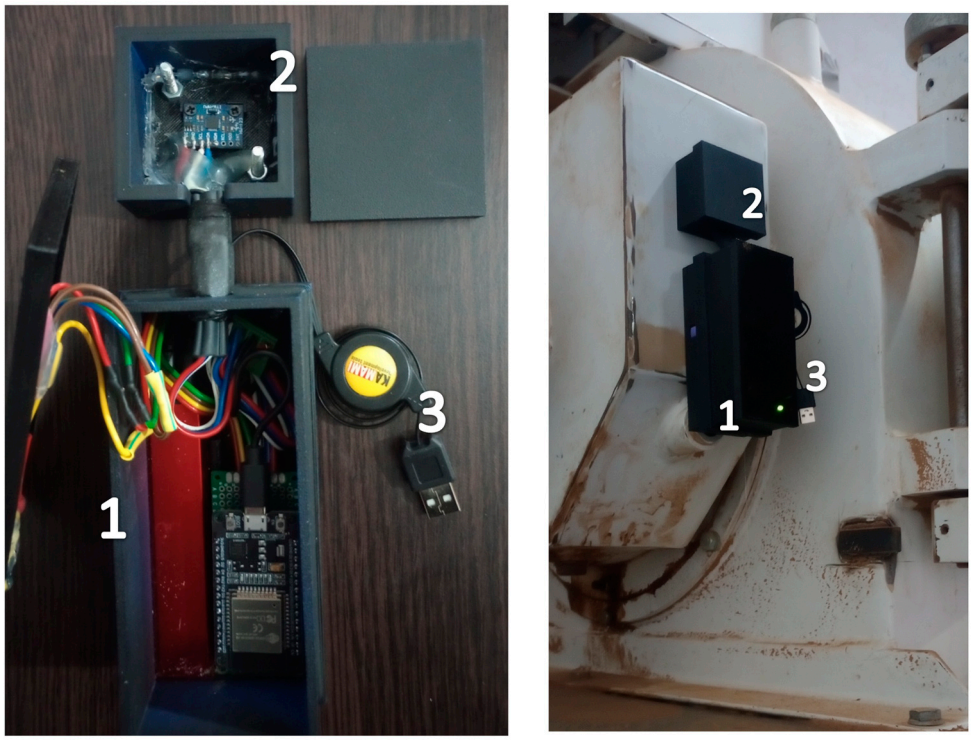


Figure 14. Access to device data through a web browser: system interface.



(**a**) (**b**)

Figure 15. (**a**) The photo of the prototype device and (**b**) its placement on the grinder housing. 1—device enclosure (ESP and power bank), 2—sensor enclosure, 3—USB cable for charging.

5. Conclusions

The study presents the results of research on the operational parameters of a needle grinder for biological materials. The focus was primarily on the wear issues of the needle elements comprising the grinder. During the operation of the device, the level and nature of the grinding system's vibrations were examined shortly after pin replacement (initial wear phase) and after grinding several hundred tons of biological material (final wear phase). A vibration signal analysis and observations of pin wear allowed for a correlation of the degradation process of both non-hardened and heat-treated pins. The conclusions from the measurements carried out with laboratory equipment led to the proposal of a low-cost prototype device using the ESP32 system and the three-axis capacitive accelerometer MPU6050.

Professional vibration measurement devices are typically portable and can be used for diagnosing various machines; however, their operation requires appropriate user expertise. The proposed device is not a universal solution but is specifically designed for a particular machine. Its main advantage is the ability to simply communicate to the operator when the working elements need replacement.

The device needs to be tested over several full production cycles (ending with the replacement of working elements) to assess its reliability and the correctness of the selected τ coefficient threshold. After verifying its performance and incorporating any feedback from the company, a final solution can be proposed.

The issue of pin wear and the associated machine vibrations may serve as a direction for further research using alternative methods, such as a visual vibration analysis with a high-speed camera, thermography, or the numerical analysis of forces acting on the working elements of the grinder.

The results obtained in the study led to the formulation of the following conclusions:

1. Regardless of the type of pins, their wear process manifests itself through an increase in the difference in accelerations in the X- and Y-axes during idle operation and grinding;
2. Pin wear also results in an increase in vibration velocity in the X-axis at a frequency of 63 Hz, corresponding to the disc's rotational speed;
3. A simple and quick assessment of pin condition in the tested machine can be performedusing a wear parameter calculated as the ratio of the difference in accelerations in the X- and Y-axes to the smaller acceleration value;
4. The vibration results obtained with laboratory equipment enabled the proposal and construction of a simple grinder monitoring tool;
5. The applied monitoring method allows for real-time and quick verification of the pin condition, thereby protecting against possible drive unit damage;
6. Microstructural studies of NC11LV steel and its hardness tests in the initial and hardened state justify the difference in the wear rate.

Author Contributions: Formal analysis, G.Ś. and M.K.; investigation, G.Ś. and M.Ł.; resources, G.Ś. and M.Ł.; data curation, G.Ś.; writing—original draft preparation, G.Ś. and M.Ł.; writing—review and editing, G.Ś. and M.K.; visualization, G.Ś.; supervision, M.K. All authors have read and agreed to the published version of the manuscript.

Funding: This research received no external funding.

Data Availability Statement: The data presented in the article are available upon request.

Acknowledgments: The authors would like to thank Krzysztof Tyszczuk and Jakub Lewandowski for their help in preparing and conducting the measurements.

Conflicts of Interest: The authors declare no conflicts of interest.

Abbreviations

The following abbreviations are used in this manuscript:

RMS Root Mean Square
IEPE Integrated Electronics Piezo-Electric

References

1. Jamwa, A.; Agrawal, R.; Sharma, M.; Giallanza, A. Industry 4.0 Technologies for Manufacturing Sustainability: A Systematic Reviewand Future Research Directions. *Appl. Sci.* **2021**, *11*, 5725. [CrossRef]
2. Ghobakhloo, M. Industry 4.0, digitization, and opportunities for sustainability. *J. Clean. Prod.* **2020**, *252*, 119869. [CrossRef]
3. Jamwal, A.; Agrawal, R.; Sharma, M.; Kumar, V.; Kumar, S. Developing A sustainability framework for Industry 4.0. *Procedia CIRP* **2021**, *98*, 430–435. [CrossRef]

4. Ramanujan, D.; Bernstein, W.Z.; Diaz-Elsayed, N.; Haapala, K.R. The Role of Industry 4.0 Technologies in Manufacturing Sustainability Assessment. *J. Manuf. Sci. Eng.* **2023**, *145*, 010801. [CrossRef]
5. Marczuk, A.; Blicharz-Kania, A.; Savinykh, P.A.; Isupov, A.Y.; Palichyn, A.V.; Ivanov, I.I. Studies of a Rotary–Centrifugal Grain Grinder Using a Multifactorial Experimental Design Method. *Sustainability* **2019**, *11*, 5362. [CrossRef]
6. Romaniuk, W.; Savinykh, P.; Borek, K.; Roman, K.; Isupov, A.Y.; Moshonkin, A.; Wałowski, G.; Roman, M. The Application of Similarity Theory and Dimensional Analysis to the Study of Centrifugal-Rotary Chopper of Forage Grain. *Energies* **2021**, *14*, 4501. [CrossRef]
7. Tyszczuk, K.; Śmigielski, G.; Domek, G. Research and modeling of operating damage to bearings in organic matter shredders. *AIP Conf. Proc.* **2023**, *2976*, 030016.
8. Pellizzari, M.; Molinari, A. The Application-Oriented Heat Treatment of Tool Steels. *Mater. Manuf. Process.* **2009**, *24*, 723–728. [CrossRef]
9. Hawryluk, M.; Lachowicz, M.M.; Marzec, J.; Nowak, K.; Suliga, M. Comparative Analysis of the Wear of NC11LV and Hardox 600 Steel Used in Tools for Extrusion of Clay Strands in the Process of Producing Ceramic Roof Tiles. *Materials* **2023**, *16*, 293. [CrossRef] [PubMed]
10. Venegas, P.; Ivorra, E.; Ortega, M.; Sáezde Ocáriz, I. Towards the Automation of Infrared Thermography Inspections for Industrial Maintenance Applications. *Sensors* **2022**, *22*, 613. [CrossRef] [PubMed]
11. Zhang, R.; Cao, Z.; Huang, Y.; Yang, S.; Xu, L.; Xu, M. Visible-Infrared Person Re-identification with Real-world Label Noise. *IEEE Trans. Circuits Syst. Video Technol.* **2025**. [CrossRef]
12. Zhang, R.; Liu, G.; Zhang, Q.; Lu, X.; Dian, R.; Yang, Y. Detail-Aware Network for Infrared Image Enhancement. *IEEE Trans. Circuits Syst. Video Technol.* **2024**. [CrossRef]
13. Hosokawa Alpine Group. Available online: https://www.hosokawa-alpine.com/powder-particle-processing/machines/fine-impact-mills/contraplex-cw-ii/ (accessed on 23 January 2025).
14. Industrial Accelerometers. Available online: https://mmf.de/wp-content/uploads/2023/11/1-10_ks74b_ks80c.pdf (accessed on 10 December 2024).
15. Handyscope HS4. Available online: https://www.tiepie.com/en/usb-oscilloscope/handyscope-hs4 (accessed on 10 December 2024).
16. NI LabVIEW. Available online: https://www.ni.com/en/shop/labview.html (accessed on 10 December 2024).
17. Folea, S. (Ed.) *Labview—Practical Applications and Solutions*; InTech: Houston, TX, USA, 2011.
18. Jabłoński, A. *Condition Monitoring Algorithms in MATLAB*; Springer: Berlin/Heidelberg, Germany, 2021.
19. Romanssini, M.; de Aguirre, P.C.C.; Compassi-Severo, L.; Girardi, A.G. A Review on Vibration Monitoring Techniques for Predictive Maintenance of Rotating Machinery. *Eng* **2023**, *4*, 1797–1817. [CrossRef]
20. Morrison, F.A. *Uncertainty Analysis for Engineers and Scientists: A Practical Guide*; Cambridge University Press: Cambridge, UK, 2021.
21. Lira, I. *Evaluating the Measurement Uncertainty: Fundamentals and Practical Guidance*; Institute of Physics Publishing: Bristol, UK, 2002.
22. Łazarska, M.; Woźniak, T.; Ranachowski, Z.; Ranachowski, P.; Trafarski, A. The Application of Acoustic Emission and Artificial Neural Networks in an Analysis of Kinetics in the Phase Transformation of Tool Steel During Austempering. *Arch. Metall. Mater.* **2017**, *62*, 603–609. [CrossRef]
23. Espressif Systems. ESP32. Available online: https://www.espressif.com/en/products/socs/esp32 (accessed on 10 December 2024).
24. InvenSense Inc. Available online: https://invensense.tdk.com (accessed on 10 December 2024).
25. Hercog, D.; Lerher, T.; Truntič, M.; Težak, O. Design and Implementation of ESP32-Based IoT Devices. *Sensors* **2023**, *23*, 6739. [CrossRef]

Disclaimer/Publisher's Note: The statements, opinions and data contained in all publications are solely those of the individual author(s) and contributor(s) and not of MDPI and/or the editor(s). MDPI and/or the editor(s) disclaim responsibility for any injury to people or property resulting from any ideas, methods, instructions or products referred to in the content.